Edaravone-Based Mononuclear Dysprosium(III) Single-Molecule Magnets

Tesfay G. Ashebr, Léo La Droitte, Xiao-Lei Li, Chen Zhao, Jinjiang Wu, Quan Zhou, Olivier Cador, Boris Le Guennic, Jinkui Tang

Edaravone based mononuclear dysprosium(III) single-molecule magnets

Tesfay G. Ashebr,[†, ‡, #] Léo La Droitte,[§] Xiao-Lei Li,[†] Chen Zhao,[†, ‡] Jinjiang Wu,[†, ‡] Quan Zhou,[†, ‡] Olivier Cador,[§] Boris Le Guennic*[, §] and Jinkui Tang*[, †, ‡]

[†]State Key Laboratory of Rare Earth Resource Utilization, Changchun Institute of Applied Chemistry, Chinese Academy of Sciences, Changchun 130022, P. R. China

[‡]School of Applied Chemistry and Engineering, University of Science and Technology of China, Hefei 230026, P. R. China

[§]Univ Rennes, CNRS, ISCR (Institut des Sciences Chimiques de Rennes) - UMR 6226, F-35000 Rennes, France

[#]Department of Industrial Chemistry, College of Applied Sciences, Addis Ababa Science and Technology University, P. O. Box 16417, Addis Ababa, Ethiopia

ABSTRACT: Using an edaravone-based aryloxide ligand, we assemble four new mononuclear Dy(III) compounds, $[Dy(L1)_2(CH_3OH)_2]\cdot Br$ (**1**); $[Dy(L1)_2(CH_3OH)_2]\cdot Cl$ (**2**); $[Dy(L1)_3(CH_3OH)(NO_3)]$ (**3**) and $[Dy(L2)_3]\cdot 2CH_3OH\cdot H_2O$ (**4**) (where L1 = methyl substituted and L2 = p-tolyl substituted ligands with NNO-tridentate coordination environments). As revealed by magneto-structural and ab initio calculations investigations, the complexes exhibited slow relaxation of the magnetization at zero applied magnetic field where their magnetic properties were

subtly tuned via chemical modifications on the dominant crystal-field (CF) interaction. For the complexes with L1 analogue under eight coordination, complexes **1** and **2** (D_{4d} symmetry) with non-coordinated halides showed better magnetic properties as compared to complex **3** (C_{2v} symmetry) due to the presence of strongly coordinated nitrate anion that leads to a change in the structural arrangement. However, complex **4** (C_{4v} symmetry) with nine coordination was found structurally unfavorable comparatively due to the coordination of an additional third ligand (L2) that leads to a higher coordination number as a result of substituent change. Therefore, the presented compounds exhibit ligands substituent as well as counter ions dependent magnetic properties variations. Relatively a higher effective energy barrier (U_{eff}) was obtained for the compounds having the halide counter anions as compared with the neutral complexes. Moreover, ab initio calculations revealed that the transition magnetic moment probabilities for these compounds present very small or even vanishing quantum tunneling of the magnetization (QTM) between the ground-state Kramers doublets (KDs), and indicate that the slow relaxation might proceed through higher excited states. Finally, the described new compounds are expected to advance the aryloxide single-molecule magnets (SMMs).

Introduction

Recently, the prospect of magnetic molecules is quite eye-catching as a result of their proposed applications as molecular qubits,[1] spin-crossover sensors,[2,3] single-molecule magnets (SMMs)[4,5] as well as molecular spintronic materials.[6] In particular, molecules possessing the ability to retain magnetization in the absence of an external magnetic field known as SMMs,[7] are expected to be potential candidates for engineering molecular spintronics.[8,9] As compared to 3*d*-based SMMs, 4*f*-based SMMs are usually associated with unrivalled magnetic anisotropy and large magnetic

moments that lead to longer relaxation times. Of the Ln(III) series, Tb(III), Dy(III), Er(III), and Ho(III) ions are among the electronic structurally favourable candidates used for assembling SMMs. More specifically, Dy(III) ion is the most popular one because i) it can be described by Kramers' theorem,[10] ii) it has a strongly oblate spheroidal shape of electron density at the ground state,[11] and iii) it has a relatively large orbital contribution to the magnetic moment.[12] Besides, less-explored lanthanide (Ce(III), Nd(III), Gd(III), Tm(II/III) and Yb(III)) single-ion magnets are also demonstrated where their recent developments summarized by Borah and co-worker.[13]

In general, high-performance Dy(III)-SMMs could be realized by employing different strategies such as CF symmetry, predominant bond, organometallic, and strong magnetic coupling approaches.[14] In particular, monomeric Dy(III) complexes designed by CF symmetry strategy such as pentagonal bipyramidal,[15–18] hexagonal bipyramidal,[19–21] and square antiprismatic,[22,23] as well as low coordinate complexes possessing predominant bond[24–28] are effective routes for pursuing high effective energy barrier (U_{eff}) and large blocking temperature (T_B). Furthermore, monomeric Dy(III) metallocenes generated from anionic cyclopentadienyl (Cp) ligands[29,30] are also proved to be high-temperature SMMs with a current record T_B of 80 K for $[(Cp^{iPr5})Dy(Cp^*)][BPh_4]$ complex where Cp^{iPr5} = penta-isopropylcyclopentadienyl, and Cp* = pentamethylcyclopentadienyl.[31] Moreover, a recent work from Long and co-workers reported $(Cp^{iPr5})_2Dy_2I_3$ complex possessing Ln-Ln bonding with a record coercive magnetic field with a lower bound of 14 tesla at 60 K.[32]

Pyrazolone, a five-membered heterocycle containing two adjacent nitrogen atoms is a powerful synthon,[33] which has been exploited widely in the development of pharmaceutical chemistry[34] and coordination chemistry[35] (e. g. magnetic exchange interaction in copper(II) complexes [36,37]). Pyrazolone-based ligands and their metal complexes have been summarized in a recent comprehensive review reported by Pettinari and co-workers.[35] To the best of our knowledge, there

is no pyrazolone-based SMM reported in the literature and we select edaravone (MCI-186, 3-methyl-1 phenyl-2-pyrazolin-5-one) which is the first known free radical scavenger[38] as a starting material (Scheme S1). Of particular relevance to the 2-(pyridin-2-yl)hydrazine grafted edaravone-based hydrazone ligands used in the present work, only two reports detailing ruthenium(II)-arene complexes and their anticancer activities are available.[39,40] In this context, we extend these ligand varieties to Dy(III) complexes to investigate their SMM behaviours. Herein, we report four mononuclear Dy(III) complexes namely, $[Dy(L1)_2(CH_3OH)_2]Br$ (**1**); $[Dy(L1)_2(CH_3OH)_2]Cl$ (**2**); $[Dy(L1)_3(CH_3OH)(NO_3)]$ (**3**) and $[Dy(L2)_3]\cdot 2CH_3OH\cdot H_2O$ (**4**). Interestingly, all complexes exhibited SMM properties at zero applied magnetic field. As confirmed by both our experimental and theoretical results, the diverse magneto-structural variations observed are attributed to the change in substituent in the edaravone-based ligands and the counter ions.

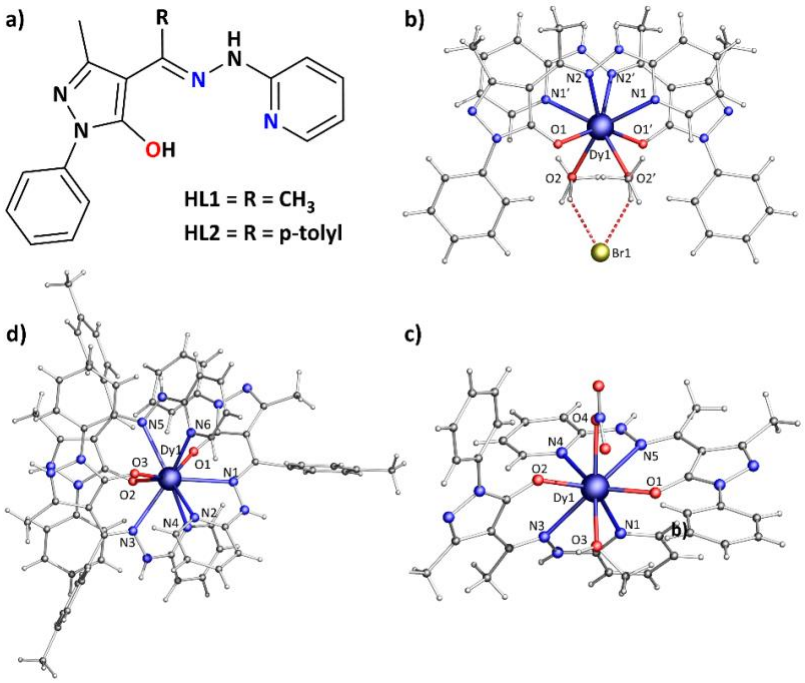

Figure 1. (a) The ligand structures of HL1 and HL2; (b-d) Crystal structures of complexes **1**, **3** and **4**. Colour codes: N, blue; O, red; Dy, deep blue; Br, yellow, C, grey and H, light grey.

Results and discussion

Structural descriptions

Under ambient conditions, the reaction of methanolic solution of HL1 and HL2 in the presence of trimethylamine with hydrated salts of Dy(III)$X_3 \cdot nH_2O$ (X = Br^-, Cl^- or NO_3^-) with 2:1 molar ratio produced block yellow crystals by diffusion with diethyl ether for **1**−**3** and slow evaporation for **4** at room temperature. It is important to note that with L1 complexes **1**−**3** were obtained with each of the different anions while for L2 same condition give only compound **4** whatever the dysprosium salt used. Single-crystal X-ray diffraction examination revealed that **1** (Figure 1) and **2** (Figure S1) crystallize in the *C*2/c space group while **3** and **4** (Figure 1) crystalize in *P*-1 and $P2_1/c$ space group, respectively (Table S1). Relatively shorter $Dy{-}O_{edaravone}$ bond distances of 2.2520(37) Å and 2.2342(17) Å were observed for **1** and **2**, respectively. In contrast, non-isotropic predominant bond distances i.e. relatively shorter $Dy_1{-}O_{1(Edaravone)}$ and $Dy_1{-}O_{2(Edaravone)}$ bond distances of 2.2062(26) Å and 2.2296(23) Å was observed respectively for **3**, while relatively larger bond distances of $Dy_1{-}O_{1(Edaravone)}$ and $Dy_1{-}O_{2(Edaravone)}$ 2.2778(30) Å and 2.2822(29) Å was observed respectively for **4** which could be attributed to the additional coordinated anionic ligand. Moreover, the $O_{edaravone}{-}Dy{-}O_{edaravone}$ bond angles of 147.56(174)°, 147.744(77)°, 131.48(9)° and 144.130(111)° were observed in **1**−**4**, respectively (Table S2). The smaller bond angle in **3** could be attributed to the presence of a strongly coordinated nitrate anion that leads to a change in the structural arrangement (Figure 1). Within the lattice, the shortest intermolecular Dy···Dy distance for **1**−**4** are 9.9726(5), 9.9684(2), 8.1225(5), and 9.4401(05) Å were observed respectively, suggesting negligible dipolar and superexchange interactions (Table S2).[41] Relatively, the larger intermolecular distance for complexes **1** and **2** could be attributed to the involvement of the halide counter ions in the crystal packing arrangement as depicted in Figure 2 (top) and Figure S2,

respectively, as compared to the neutral complexes **3** and **4** as shown in Figure S3 and Figure 2 (bottom) respectively.

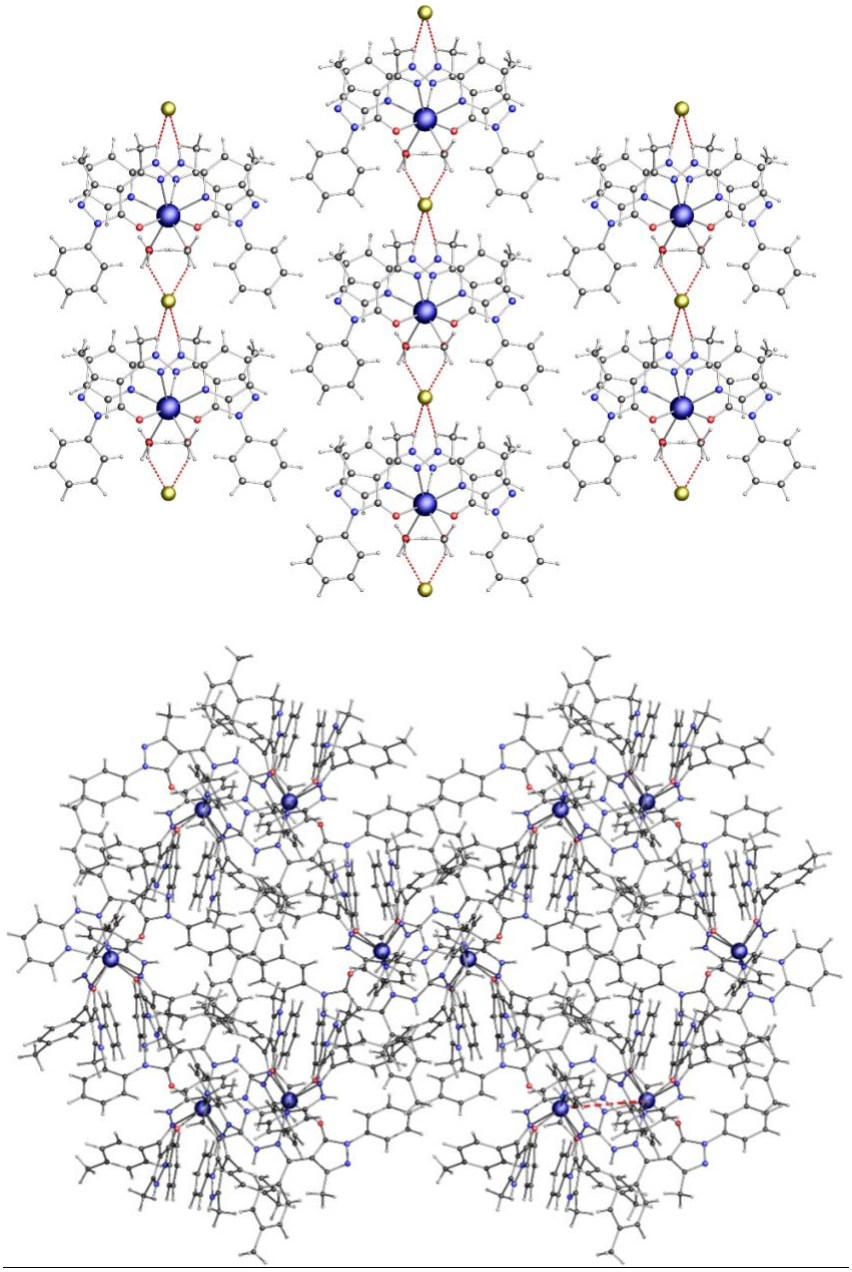

Figure 2. Crystal packing arrangement of complexes **1** and **4**. Colour codes: N, blue; O, red; Dy, deep blue; Br, yellow; C, grey and H, light grey. Dashed red lines indicate hydrogen bonding and shortest Dy···Dy bond distances of complexes **1** and **4** respectively.

According to SHAPE analysis for the geometric symmetry of the first coordination sphere of Dy(III) ion,[42,43] the D_{4d} symmetry (square antiprism) for **1** and **2** and C_{2v} symmetry (bi-augmented trigonal prism) for **3** as well as C_{4v} symmetry (spherical capped square antiprism) for **4** were confirmed (Figure 3 & Table S3). In comparison, complexes **1** and **2** are almost identical while a considerable structural difference was observed for complex **3** that could be attributed to the nitrate ion coordination creating potential stress on the entire structural arrangement. However, the coordination number switching from 8 to 9 was observed upon treatment of L2 with a variation of Dy(III) salts under the same reaction conditions as **1**−**3**. This event was initiated by changing the substituent in the starting material edaravone-based ligand, i.e. the *p*-tolyl substituted L2 favors a higher coordination number while methyl-substituted L1 stabilizes a lower coordination number.

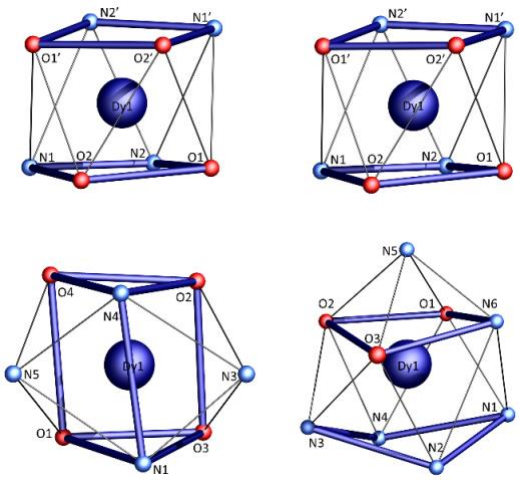

Figure 3. Coordination polyhedrons observed in **1**−**4**.

Magnetic properties

Temperature-dependent direct current (dc) magnetic susceptibility ($\chi_M T$, χ_M is the molar magnetic susceptibility) investigations have been done at a temperature range of 1.9−300 K under dc field of 1 kOe for all complexes. Accordingly, $\chi_M T$ values of 13.64, 13.72, 14.09, and 14.14 cm^3 K

mol^{-1} at 300 K are obtained for complexes **1−4**, respectively (Figure S4). These results are comparable with the expected value of 14.17 cm^3 K mol^{-1} for a free Dy(III) ion (S = 5/2, L = 5, g = 4/3 and $^6H_{15/2}$). The $\chi_M T$ values gradually decrease upon lowering the temperature followed by dropping to minimal values at a lower temperature (below 20 K) in all complexes could be ascribed to the progressive quenching of excited Stark-sublevels of Dy(III) ion and the occurrence of weaker intermolecular interactions. Field-dependent magnetization of all complexes was studied in the field range of 0−7 T at 1.9, 3.0 and 5.0 K. The saturated magnetization values vary from 5.48 to 6.68 μ_B for **1−4**. Remarkably, complexes **1−3** also displayed well-defined butterfly-shaped hysteresis loops at 1.9 K except for complex **4** evidencing the impact of substituent change in the edaravone-based ligand and the counter ions that lead to diverse magneto-structural variations (Figure S11).

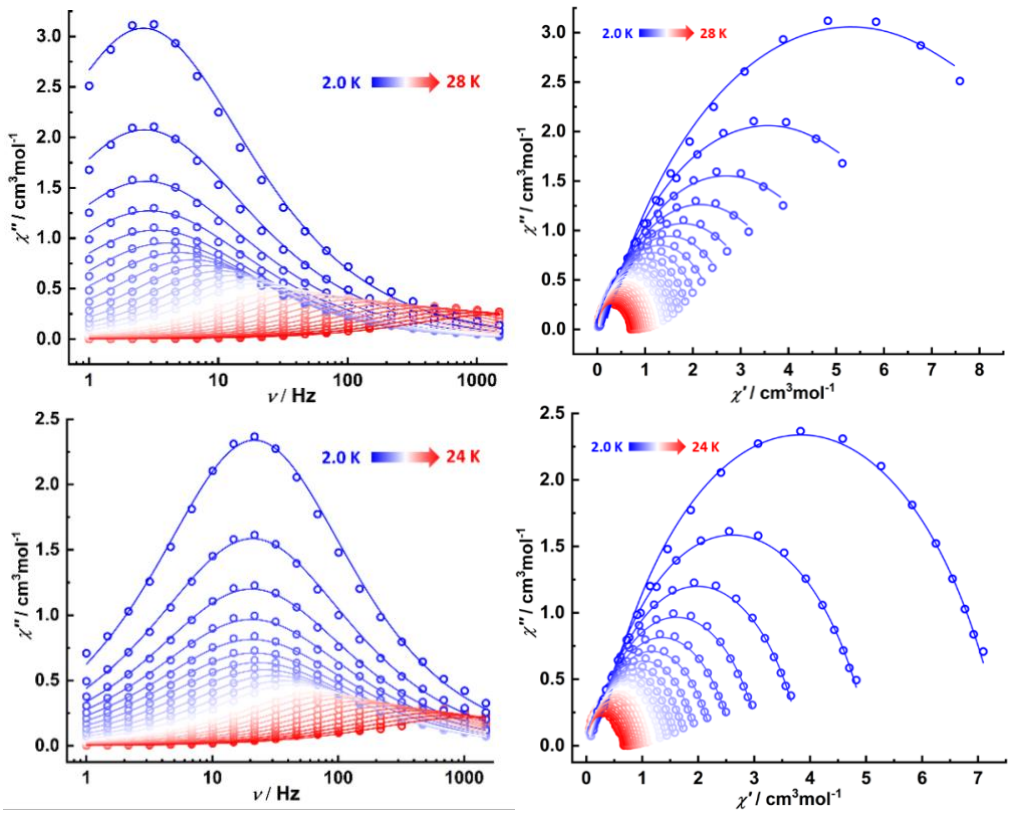

Figure 4. Frequency-dependent out-of-phase (χ'') and Cole−Cole plots for **1** (top) and **2** (bottom) where solid lines are generalized Debye fits.

To probe the magnetization dynamics, alternating current (ac) magnetic susceptibility measurements were performed using an oscillating field of 3 Oe and a zero dc field for **1**−**4**. All complexes exhibited frequency- and temperature-dependant ac signals typical of SMM behaviour with well-defined out-of-phase signal (χ'') maxima for **1**−**3** (Figure 4, Figures S5 and S7-S9), but weak shoulder peaks for **4** (Figure S6). The results indicate that the SMM properties depend strongly on their coordination geometry because of different ligands and counter ions variations. To investigate the impact of dilution study for potential magnetic properties improvement of the structurally unfavourable complex **4**, magnetically diluted sample **4** (1:9 ratio of Dy and Y), named **4@Y** confirmed by cross-checking the unit cell with its respective undiluted counterpart was also conducted. Significant magnetic properties enhancement was observed for **4@Y** (Figure S10),

implying that the dipole-dipole interactions in complex **4@Y** were effectively suppressed (Figure S3b) (Note: magnetic dilution study for complexes of **2** and **3** was neglected as preliminary dilution test do not show significant magnetic properties improvement as compared with their respective none-diluted samples). Moreover, well-defined frequency-dependent Cole-Cole plots of **1** and **2** (Figure 4) **3** and **4@Y** (Figures S9 and S10) obtained by fitting the measurement data to a generalized Debye model displayed non-symmetrical semicircles affirming the one-step relaxation process of magnetization.[44]

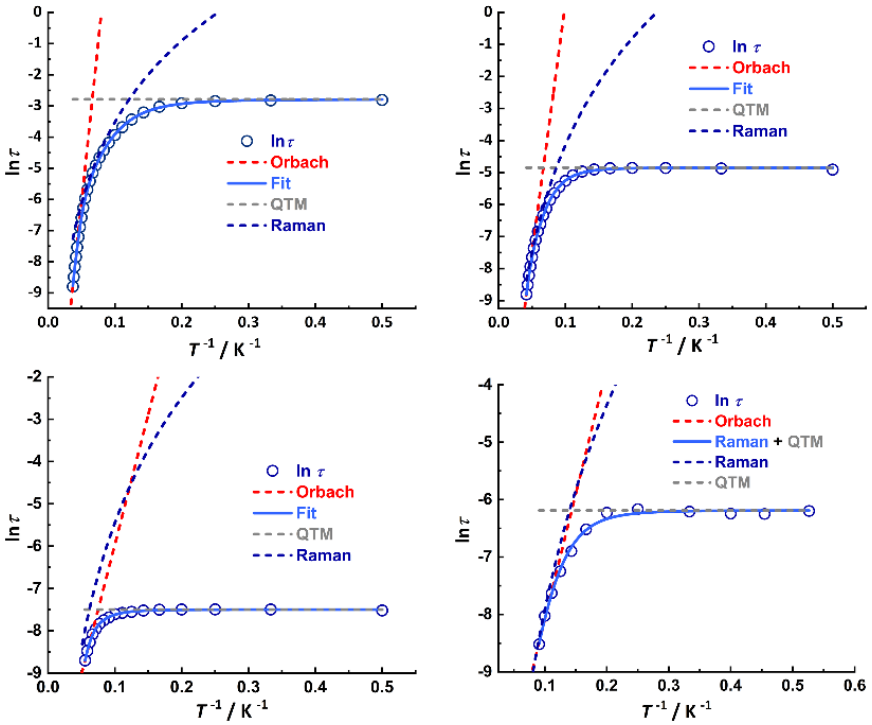

Figure 5. The lnτ vs. T^{-1} plots. Top; left for **1** and right for **2**. Bottom; left for **3** and right for **4@Y** under zero dc-field. The lnτ vs. T^{-1} plots were fitted using equation $\ln\tau = -\ln[B + CT^n + \tau_0^{-1}\exp(-U_{eff}/k_BT)]$[45] considering QTM (B), Raman (CT^n) and Orbach processes.

To evaluate the effective energy barrier (U_{eff}), relaxation times (τ) were obtained by fitting the measurements to a generalized Debye model using CC-FIT2 for **1**–**3** and **4@Y** (Figure 5).[44] Based

on our fitting results the U_{eff} (cm^{-1}) and τ_0 (s) are; 164.14 (3), 3.17 (4) × 10^{-8} for **1** (C = 5.77 × 10^{-3} s^{-1} $K^{-3.76}$; n = 3.76; B = 16.23); 207.64 (38), 1.69 (2) × 10^{-9} for **2** (C = 9.6 × 10^{-4} s^{-1} $K^{-4.82}$; n = 4.82; B = 127.75); 131.11 (41), 2.05(4) × 10^{-8} for **3** (C = 0.0125 s^{-1} $K^{-4.27}$; n = 4.27; B = 1803.26), respectively. Notably, no clear linear region for **4@Y** is observed. Fitting of τ to an Orbach model of the form $\ln\tau = -\ln[\tau_0^{-1}\exp(-U_{eff}/k_BT)]$ yields U_{Orbach} = 30.4 cm^{-1} and $\tau_0 = 3.85 \times 10^{-6}$ s. However, ab initio calculation results show that the energy of the first excited Kramers doublet of **4@Y** is at 116 cm^{-1} (vide infra), which is about four times larger than the energy barrier U_{Orbach}. The discrepancy between experimental and theoretical energy barriers indicates that Orbach relaxation mechanism is less relevant. Therefore, in order to fit the curves more reasonably and give better fitting parameters, the equation $\ln\tau = -\ln[B + CT^m]$ that only contains QTM and Raman terms was employed to fit the plot of **4@Y**. Fitting of the complete temperature-range data of **4@Y** to a sum of QTM and Raman laws dominating at low and high temperature region, respectively affords B = 487.09 (low temperature), C = 0.02 s^{-1} $K^{-5.14}$ m = 5.14 (high temperature). Complexes **1** and **2** have relatively higher U_{eff} values benefiting from their geometric symmetry of D_{4d} with shorter Dy−O bond distances and larger O−Dy−O bond angle (Tables S2 and S3) while a lower U_{eff} for **4@Y** is observed as another anionic ligand coordination leads to the increase of equatorial CF. Similarly, complex **3** also showed a lower U_{eff} than **1** and **2** as the strongly coordinated nitrate ion could weaken the dominant component of the CF induced by Dy−O bonds. According to the obtained results, the magnetic properties variations are attributed to the changes in ligands substituent as well as counter ions leading to the comparison pattern of the complexes **2** > **1** > **3** > **4**. The slightly higher U_{eff} of **2** as compared to **1** could be due to its relatively shorter $Dy-O_{edaravone}$ bond distances and larger $O_{edaravone}-Dy-O_{edaravone}$ bond angle (Table S2).[46]

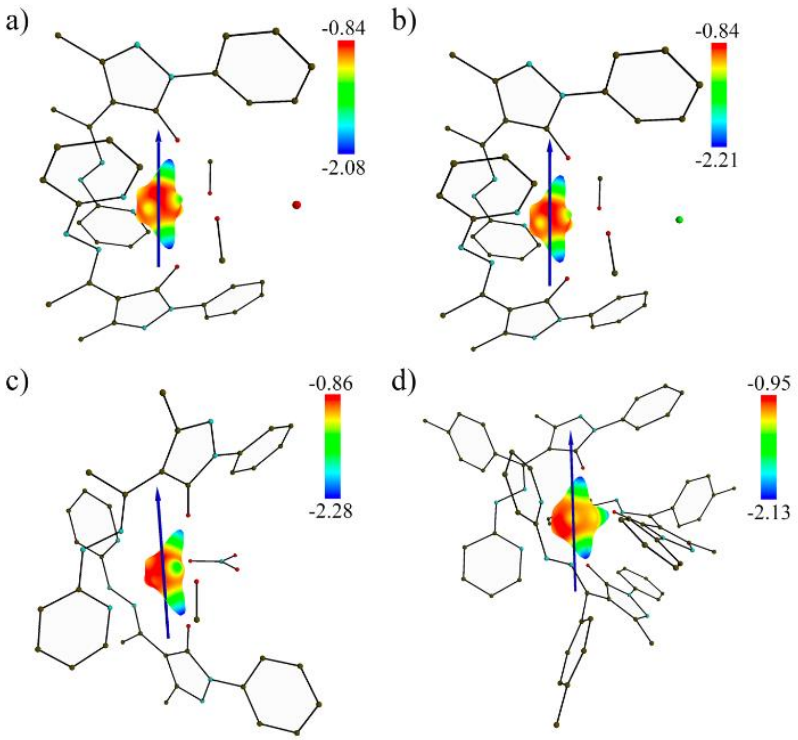

Figure 6. Calculated total electrostatic potentials (expressed in e^{-} $bohr^{-1}$) at 3 Å around the Dy(III) ion with the gz direction in blue arrow for compounds **1** (a), **2** (b), **3** (c) and **4** (d). Color code: grey = C; cyan = N; red = O; brown = Br and green = Cl.

Ab initio calculations

Quantum chemical calculations have been performed at the SA-CASSCF/RASSI-SO level on the X-ray crystal structures for each compound (see computational details). For **1** and **2**, two sets of calculations were carried out to study the impact of the counter ion on the computed wavefunction, i.e. with or without considering the counter ion (Br^{-} or Cl^{-}) in the computed structure. As seen in Figure S14 and Tables S8−11, the presence of the counter ion in the calculation, while quite close to the paramagnetic centre does not influence drastically the calculated properties. An overall good agreement with the experimental $\chi_M T$ data is found at high temperature for all the four compounds, while the important decrease observed at low temperature is not computationally reproduced (Figure S4). The ground Kramers Doublets (KDs) are almost

pure $m_J = |\pm 15/2>$ for the four compounds (Tables S8-S13) and as shown in Figure 6, the main component of the ***g*** tensor is as expected mainly driven by the negative electrostatic potential of the two oxygen atoms from the edaravone moiety of the two ligands (L1 & L2). The overall splitting of the $^6H_{15/2}$ ground states of **1**, **2,** and **3** are 576, 642, and 635 cm^{-1} respectively, while it is about 442 cm^{-1} for **4**. The first excited state, mainly $m_J = |\pm 13/2>$, is at 180, 194, and 154 cm^{-1} for **1**, **2,** and **3** respectively, while it is at 116 cm^{-1} for **4**. These differences between **4** and the other three compounds could find an explanation in the shape of the crystal field created by the three L2 ligands surrounding the Dy(III) ion, which seems to be slightly more spherical than the crystal field formed by two L1 ligands coordinated to a Dy(III) ion. The transition magnetic moment probabilities for these compounds (Figure 7 and Figure S15) present very small or even vanishing QTM between the ground-state KDs, and indicate that the slow relaxation might proceed through higher excited states (thermally activated mechanisms).

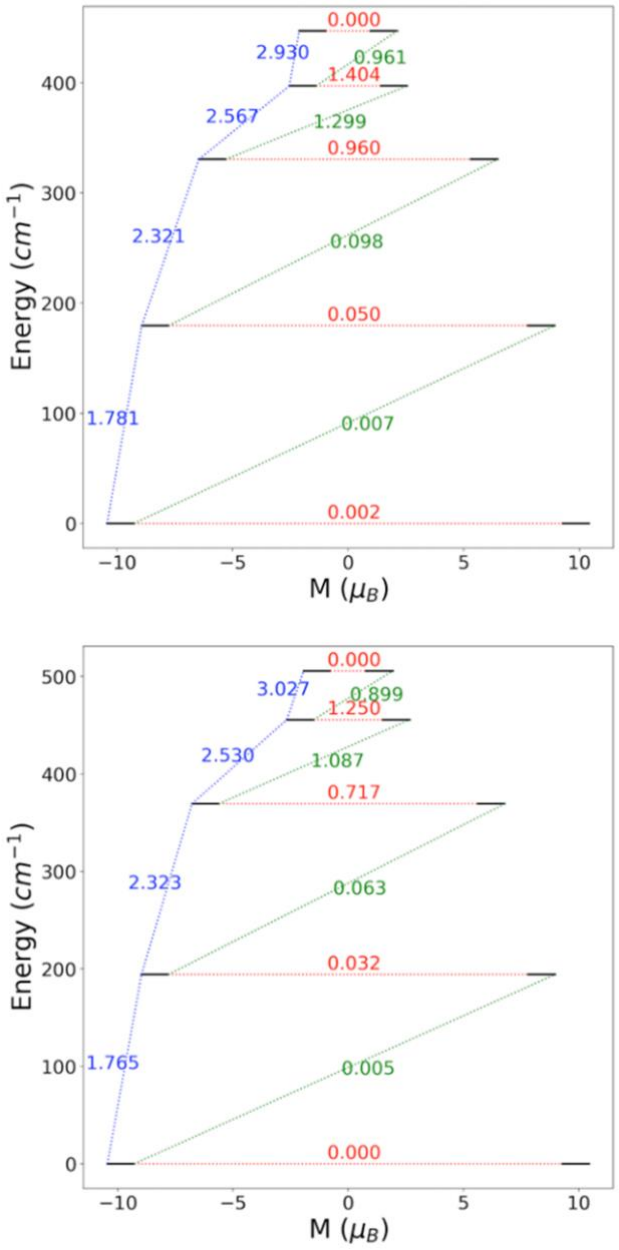

Figure 7. Calculated magnetization blocking barrier of the Dy center for the compounds **1** (top), and **2** (bottom). Only the fifth lowest KDs (thick black lines) are represented according to their magnetic moment along the main magnetic axis. The blue dashed lines represent vertical excitations, the green dashed lines correspond to possible Orbach relaxation processes while the red dashed lines correspond to QTM/TA-QTM processes. The values correspond to the mean value of the corresponding transversal matrix element of the transition magnetic moment.

Conclusions

In summary, we report first typical examples of edaravone-based mononuclear Dy(III) compounds in which their magnetic properties were subtly tuned through chemical modifications on the dominant crystal-field interaction (Figure 6). Hence, as per our experimental and computed results, the complexes with halide counter ions (**1** and **2**) benefited from their structural arrangement to exhibit relatively better magnetic properties. While the reverse event was observed for the neutral complexes which could be attributed to; i) the potential stress on the predominant bond strength as a result of the coordinated nitrate counter ion in **3** and ii) the involvement of additional anionic ligand coordination initiated by substituent change in the ligand which ends up with a magnetically unfavourable spherical structure in **4**. Finally, we believe, the present new family are expected to advance the aryloxide SMMs.[47]

Experimental

All solvents and chemicals were of analytical grade and used without further purification. All reactions were also carried out under ambient conditions. Magnetic susceptibility measurements of polycrystalline samples were carried out in the temperature range of 1.9−300 K using a Quantum Design MPMS-XL7 SQUID magnetometer equipped with a 7 T magnet. Single crystals were mounted on glass fibers and diffraction data were obtained via a Bruker AXS D8 Venture single-crystal diffractometer equipped with graphite monochromatized Mo Kα (λ = 0.71073) at corresponding temperatures. The precursor edaravone-based ketones namely; 1-(5-hydroxy-3-methyl-1-phenyl-1H-pyrazole-4-yl)ethanone and (5-hydroxy-3-methyl-1-phenyl-1H-pyrazole-4-yl)(p-tolyl)methanone were synthesized using the Jensen method.[48] Ligands HL1 (56% yield) and HL2 (63% yield) were synthesized as previously reported procedure[39] (Scheme S1). ^{1}HNMR

($CDCl_3$, 400 MHz, 300 K); 8.23 (m, 1H, amine −NH), 7.98 (m, 1H, pyridyl −H), 7.39 (m, 4H, aromatic −H), 7.18 (m, 1H, pyridyl −H), 6.92 (d, 2H, pyridyl −H), 2.52 (s, 3H, pyrazole $-CH_3$), 2.48 (s, 3H, acyl$-CH_3$) for HL1 as well as ^{1}HNMR ($CDCl_3$, 400 MHz, 300 K); 8.14 (m, 1H, amine −NH), 7.64 (m, 1H, pyridyl −H), 7.47 (m, 4H, aromatic −H), 7.32 (m, 2H, tolyl −H), 7.24 (m, 2H, tolyl −H), 7.03 (m, 1H, pyridyl −H), 6.86 (d, 2H, pyridyl −H), 2.46 (s, 3H, pyrazolyl $-CH_3$), 1.67 (s, 3H, tolyl $-CH_3$) for HL2, respectively.

General synthesis of complexes. All complexes are synthesized under similar condition. To a 0.2 mmol concentration in 10 mL methanol of L1 and L2 solution, a 0.1 mmol of Dy(III)$X_3.nH_2O$ were added under 2:2:1 ligand, base and metal molar ratio. After 10−20 minutes stirring under ambient conditions, all the reactions were filtered. Diffusion under diethyl ether for about three weeks for the filtrates of L1 analogues were isolated as colorless block crystals for $[Dy(L1)_2(CH_3OH)_2]Br$ (**1**), $[Dy(L1)_2(CH_3OH)_2]Cl$ (**2**) and light yellow block crystals for $[Dy(L1)_3(CH_3OH)(NO_3)]$ (**3**) while a slow evaporation for a week for L2 analogue was isolated as yellow block crystals $[Dy(L2)_3]\cdot 2CH_3OH\cdot H_2O$ (**4**) in 42, 48, 59 and 73% yield based on Dy(III) respectively. It is important to note that under similar reaction conditions and molar ratio, treatment of Dy(III) salts with Br^-, Cl^- and NO_3^- counter anions with L2 was isolated as a neutral isostructural complex **4**. Complex **4@Y** with 51% yield (1:9 ratio of Dy(III) and Y(III) salts) was also synthesized in similar procedure for magnetic dilution study. To ensure purity of the complexes, collected crystals were thoroughly washed by methanol and diethyl ether before any characterization. Elemental analysis (%) calcd for $C_{36}H_{40}BrDyN_{10}O_4$ (MW = 919.18); C, 47.04, H, 4.39, N, 15.24; found C, 47.06, H, 4.40, N, 15.22 and FT-IR υ/cm^{-1} (ATR): 3191 (m), 1566 (s), 1461 (s), 1000 (m), 957 (m), 755 (vs), 619 (m), 552 (s) for **1**; $C_{36}H_{40}ClDyN_{10}O_4$ (MW = 874.73); C, 49.43, H, 4.61, N, 16.01; found C, 49.46, H, 4.62, N, 16.02 and FT-IR υ/cm^{-1} (ATR): 3189 (m),

1562 (s), 1459 (s), 998 (m), 949 (m), 751 (vs), 617 (m), 549 (s) for **2**; $C_{35}H_{36}DyN_{11}O_6$ (MW = 869.25); C, 48.36, H, 4.17, N, 17.73; found C, 48.36, H, 4.15, N, 17.72 and FT-IR υ/cm^{-1} (ATR): 3251 (m), 1559 (s), 1458 (s), 996 (m), 947 (m), 746 (vs), 615 (m), 547 (s) for **3**; and $C_{71}H_{70}DyN_{15}O_6$ (MW = 1391.92); C, 61.26, H, 5.07, N, 15.09; found C, 61.28, H, 5.05, N, 15.12 and FT-IR υ/cm^{-1} (ATR): 3282 (m), 1557 (s), 1456 (s), 994 (m), 944 (m), 745 (vs), 613 (m), 545 (s) for **4** respectively. Thermogravimetric and powder X-ray diffraction results of all complexes are also provided in Figures S12 & S13.

ASSOCIATED CONTENT

Supporting Information

The Supporting Information is available free of charge on the ACS Publications website at DOI: Experimental Scheme, the crystallographic data, shape analysis, magnetic measurements, IR spectroscopy of complexes, Thermogravimetric analysis of complexes, relaxation fitting parameters, and *Ab initio* calculations.

Accession Codes

CCDC 2120042−2120045 contains the supplementary crystallographic data for this paper. These data can be obtained free of charge via www.ccdc.cam.ac.uk/data_request/cif, or by contacting The Cambridge Crystallographic Data Centre, 12 Union Road, Cambridge CB2 1EZ, UK; fax: +44 1223 336033.

AUTHOR INFORMATION

Corresponding Authors

Jinkui Tang − *State Key Laboratory of Rare Earth Resource Utilization, Changchun Institute of Applied Chemistry, Chinese Academy of Sciences, Changchun 130022, P. R. China; University of Science and Technology of China, Hefei 230026, P. R. China; https://orcid.org/0000-0002-8600-7718; Email: tang@ciac.ac.cn*

Boris Le Guennic − *Univ Rennes, CNRS, ISCR (Institut des Sciences Chimiques de Rennes) - UMR 6226, F-35000 Rennes, France. E-mail: boris.leguennic@univ-rennes1.fr*

Authors

Tesfay G. Ashebr − *State Key Laboratory of Rare Earth Resource Utilization, Changchun Institute of Applied Chemistry, Chinese Academy of Sciences, Changchun 130022, P. R. China; University of Science and Technology of China, Hefei 230026, P. R. China; Department of Industrial Chemistry, College of Applied Sciences, Addis Ababa Science and Technology University, P. O. Box 16417, Addis Ababa, Ethiopia*

Léo La Droitte − *Univ Rennes, CNRS, ISCR (Institut des Sciences Chimiques de Rennes) - UMR 6226, F-35000 Rennes, France*

Xiao-Lei Li − *State Key Laboratory of Rare Earth Resource Utilization, Changchun Institute of Applied Chemistry, Chinese Academy of Sciences, Changchun 130022, P. R. China*

Chen Zhao − *State Key Laboratory of Rare Earth Resource Utilization, Changchun Institute of Applied Chemistry, Chinese Academy of Sciences, Changchun 130022, P. R. China; University of Science and Technology of China, Hefei 230026, P. R. China*

Jinjiang Wu − *State Key Laboratory of Rare Earth Resource Utilization, Changchun Institute of Applied Chemistry, Chinese Academy of Sciences, Changchun 130022, P. R. China; University of Science and Technology of China, Hefei 230026, P. R. China*

Quan Zhou − *State Key Laboratory of Rare Earth Resource Utilization, Changchun Institute of Applied Chemistry, Chinese Academy of Sciences, Changchun 130022, P. R. China; University of Science and Technology of China, Hefei 230026, P. R. China*

Olivier Cador − *Univ Rennes, CNRS, ISCR (Institut des Sciences Chimiques de Rennes) - UMR 6226, F-35000 Rennes, France*

Notes

The authors declare no competing financial interest.

Acknowledgments

We thank the Key Research Program of Frontier Sciences, CAS (ZDBS-LY-SLH023), the Key Research Program of the Chinese Academy of Sciences (ZDRW-CN-2021-3-3), the National Natural Science Foundation of China (21871247) and the National Science and Technology Major Project (2020YFE0204500) for financial support. J. T. gratefully acknowledges the support of the Royal Society-Newton Advanced Fellowship (NA160075). T. G. A. also thankfully acknowledges CAS-TWAS President's Fellowship Program for his PhD study sponsorship. L. L. D. and B. L. G. thanks the French GENCI/IDRIS-CINES centres for high-performance computing resources. L. L. D. acknowledges the ANR (French National Research Agency) under project number ANR-19-CE07-0019-1 for PhD financial support.

References

(1) Gaita-Ariño, A.; Luis, F.; Hill, S.; Coronado, E. Molecular Spins for Quantum Computation. *Nat. Chem.* **2019**, *11*, 301–309.

(2) Brooker, S. Spin Crossover with Thermal Hysteresis: Practicalities and Lessons Learnt. *Chem. Soc. Rev.* **2015**, *44*, 2880–2892.

(3) Gebretsadik, T.; Yang, Q.; Wu, J.; Tang, J. Hydrazone Based Spin Crossover Complexes: Behind the Extra Flexibility of the Hydrazone Moiety to Switch the Spin State. *Coord. Chem. Rev.* **2021**, *431*, 213666.

(4) Liddle, S. T.; Van Slageren, J. Improving *f*-Element Single Molecule Magnets. *Chem. Soc. Rev.* **2015**, *44*, 6655–6669.

(5) Zhu, Z.; Guo, M.; Li, X. L.; Tang, J. Molecular Magnetism of Lanthanide: Advances and Perspectives. *Coord. Chem. Rev.* **2019**, *378*, 350–364.

(6) Coronado, E. Molecular Magnetism: From Chemical Design to Spin Control in Molecules, Materials and Devices. *Nat. Rev. Mater.* **2020**, *5*, 87–104.

(7) Sessoli, R.; Gatteschi, D.; Caneschi, A.; Novak, M. A. Magnetic Bistability in a Metal-Ion Cluster. *Nature* **1993**, *365*, 141–143.

(8) Vincent, R.; Klyatskaya, S.; Ruben, M.; Wernsdorfer, W.; Balestro, F. Electronic Read-out of a Single Nuclear Spin Using a Molecular Spin Transistor. *Nature* **2012**, *488*, 357–360.

(9) Shiddiq, M.; Komijani, D.; Duan, Y.; Gaita-Ariño, A.; Coronado, E.; Hill, S. Enhancing Coherence in Molecular Spin Qubits via Atomic Clock Transitions. *Nature* **2016**, *531*, 348–351.

(10) Klein, M. J. On a Degeneracy Theorem of Kramers. *Am. J. Phys.* **1952**, *20*, 65–71.

(11) Rinehart, J. D.; Long, J. R. Exploiting Single-Ion Anisotropy in the Design of *f*-Element

Single-Molecule Magnets. *Chem. Sci.* **2011**, *2*, 2078–2085.

(12) Day, B. M.; Guo, F. S.; Layfield, R. A. Cyclopentadienyl Ligands in Lanthanide Single-Molecule Magnets: One Ring to Rule Them All? *Acc. Chem. Res.* **2018**, *51*, 1880–1889.

(13) Borah, A.; Murugavel, R. Magnetic Relaxation in Single-Ion Magnets Formed by Less-Studied Lanthanide Ions Ce(III), Nd(III), Gd(III), Ho(III), Tm(II/III) and Yb(III). *Coord. Chem. Rev.* **2022**, *453*, 214288.

(14) Ashebr, T. G.; Li, H.; Ying, X.; Li, X.; Zhao, C.; Liu, S.; Tang, J. Emerging Trends on Designing High- Performance Dysprosium(III) Single-Molecule Magnets. *ACS Mater. Lett.* **2022**, *4*, 307–319.

(15) Ding, Y. S.; Chilton, N. F.; Winpenny, R. E. P.; Zheng, Y. Z. On Approaching the Limit of Molecular Magnetic Anisotropy: A Near-Perfect Pentagonal Bipyramidal Dysprosium(III) Single-Molecule Magnet. *Angew. Chem. Int. Ed.* **2016**, *55*, 16071–16074.

(16) Liu, J.; Chen, Y. C.; Liu, J. L.; Vieru, V.; Ungur, L.; Jia, J. H.; Chibotaru, L. F.; Lan, Y.; Wernsdorfer, W.; Gao, S.; Chen, X. M.; Tong, M. L. A Stable Pentagonal Bipyramidal Dy(III) Single-Ion Magnet with a Record Magnetization Reversal Barrier over 1000 K. *J. Am. Chem. Soc.* **2016**, *138*, 5441–5450.

(17) Canaj, A. B.; Dey, S.; Wilson, C.; Céspedes, O.; Rajaraman, G.; Murrie, M. Engineering Macrocyclic High Performance Pentagonal Bipyramidal Dy(III) Single-Ion Magnets. *Chem. Commun.* **2020**, *56*, 12037–12040.

(18) Sutter, J.-P.; Béreau, V.; Jubault, V.; Bretosh, K.; Pichon, C.; Duhayon, C. Magnetic Anisotropy of Transition Metal and Lanthanide Ions in Pentagonal Bipyramidal Geometry. *Chem. Soc. Rev.* **2022**, *51*, 3280–3313.

(19) Canaj, A. B.; Dey, S.; Martí, E. R.; Wilson, C.; Rajaraman, G.; Murrie, M. Insight into D_{6h}

Symmetry: Targeting Strong Axiality in Stable Dysprosium(III) Hexagonal Bipyramidal Single-Ion Magnets. *Angew. Chem. Int. Ed.* **2019**, *58*, 14146–14151.

(20) Zhu, Z.; Zhao, C.; Feng, T.; Liu, X.; Ying, X.; Li, X. L.; Zhang, Y. Q.; Tang, J. Air-Stable Chiral Single-Molecule Magnets with Record Anisotropy Barrier Exceeding 1800 K. *J. Am. Chem. Soc.* **2021**, *143*, 10077–10082.

(21) Li, Z. H.; Zhai, Y. Q.; Chen, W. P.; Ding, Y. S.; Zheng, Y. Z. Air-Stable Hexagonal Bipyramidal Dysprosium(III) Single-Ion Magnets with Nearly Perfect D_{6h} Local Symmetry. *Chem. Eur. J.* **2019**, *25*, 16219–16224.

(22) Bala, S.; Huang, G. Z.; Ruan, Z. Y.; Wu, S. G.; Liu, Y.; Wang, L. F.; Liu, J. L.; Tong, M. L. A Square Antiprism Dysprosium Single-Ion Magnet with an Energy Barrier over 900 K. *Chem. Commun.* **2019**, *55*, 9939–9942.

(23) Wu, J.; Jung, J.; Zhang, P.; Zhang, H.; Tang, J.; Le Guennic, B. *Cis-trans* Isomerism Modulates the Magnetic Relaxation of Dysprosium Single-Molecule Magnets. *Chem. Sci.* **2016**, *7*, 3632–3639.

(24) Wang, C.; Sun, R.; Chen, Y.; Wang, B. W.; Wang, Z. M.; Gao, S. Assembling High-Temperature Single-Molecule Magnets with Low-Coordinate Bis(Amido) Dysprosium Unit $[DyN_2]^+$ via Cl-K-Cl Linkage. *CCS Chem.* **2020**, *2*, 362–368.

(25) Zhu, Z.; Zhang, Y.-Q.; Li, X.-L.; Guo, M.; Lu, J.; Liu, S.; Layfield, R. A.; Tang, J. Tuning Magnetic Relaxation in Square-Pyramidal Dysprosium Single-Molecule Magnets Using Apical Alkoxide Ligands. *CCS Chem.* **2021**, *3*, 388–398.

(26) Harriman, K. L. M.; Brosmer, J. L.; Ungur, L.; Diaconescu, P. L.; Murugesu, M. Pursuit of Record Breaking Energy Barriers: A Study of Magnetic Axiality in Diamide Ligated Dy^{III} Single-Molecule Magnets. *J. Am. Chem. Soc.* **2017**, *139*, 1420–1423.

(27) Liu, B. C.; Ge, N.; Zhai, Y. Q.; Zhang, T.; Ding, Y. S.; Zheng, Y. Z. An Imido Ligand Significantly Enhances the Effective Energy Barrier of Dysprosium(III) Single-Molecule Magnets. *Chem. Commun.* **2019**, *55*, 9355–9358.

(28) Thomas-Hargreaves, L. R.; Hunger, D.; Kern, M.; Wooles, A. J.; Van Slageren, J.; Chilton, N. F.; Liddle, S. T. Insights into: D_{4h}@metal-Symmetry Single-Molecule Magnetism: The Case of a Dysprosium-Bis(Boryloxide) Complex. *Chem. Commun.* **2021**, *57*, 733–736.

(29) Goodwin, C. A. P.; Ortu, F.; Reta, D.; Chilton, N. F.; Mills, D. P. Molecular Magnetic Hysteresis at 60 Kelvin in Dysprosocenium. *Nature* **2017**, *548*, 439–442.

(30) Randall McClain, K.; Gould, C. A.; Chakarawet, K.; Teat, S. J.; Groshens, T. J.; Long, J. R.; Harvey, B. G. High-Temperature Magnetic Blocking and Magneto-Structural Correlations in a Series of Dysprosium(III) Metallocenium Single-Molecule Magnets. *Chem. Sci.* **2018**, *9*, 8492–8503.

(31) Guo, F. S.; Day, B. M.; Chen, Y. C.; Tong, M. L.; Mansikkamäki, A.; Layfield, R. A. Magnetic Hysteresis up to 80 Kelvin in a Dysprosium Metallocene Single-Molecule Magnet. *Science* **2018**, *362*, 1400–1403.

(32) Gould, C. A.; McClain, K. R.; Reta, D.; Kragskow, J. G. C.; Marchiori, D. A.; Lachman, E.; Choi, E. S.; Analytis, J. G.; Britt, R. D.; Chilton, N. F.; Harvey, B. G.; Long, J. R. Ultrahard Magnetism from Mixed-Valence Dilanthanide Complexes with Metal-Metal Bonding. *Science* **2022**, *375*, 198–202.

(33) Liu, S.; Bao, X.; Wang, B. Pyrazolone: A Powerful Synthon for Asymmetric Diverse Derivatizations. *Chem. Commun.* **2018**, *54*, 11515–11529.

(34) Adhikari, S.; Singh, M.; Sharma, P.; Arora, S. Pyrazolones as a Potential Anticancer Scaffold: Recent Trends and Future Perspectives. *J. Appl. Pharm. Sci.* **2021**, *11*, 26–37.

(35) Marchetti, F.; Pettinari, C.; Di Nicola, C.; Tombesi, A.; Pettinari, R. Coordination Chemistry of Pyrazolone-Based Ligands and Applications of Their Metal Complexes. *Coord. Chem. Rev.* **2019**, *401*, 213069.

(36) Popov, L. D.; Levchenkov, S. I.; Shcherbakov, I. N.; Minin, V. V.; Aleksandrov, G. G.; Ugolkova, E. A.; Lukov, V. V.; Kogan, V. A. Polymeric Copper(II) Complexes with 4-Formyl-3-Methyl-1-Phenylpyrazol-5-One Hetarylhydrazones: Synthesis and Crystal Structures. *Russ. J. Coord. Chem.* **2013**, *39*, 849–856.

(37) Levchenkov, S. I.; Shcherbakov, I. N.; Popov, L. D.; Lukov, V. V.; Minin, V. V.; Starikova, Z. A.; Ivannikova, E. V.; Tsaturyan, A. A.; Kogan, V. A. The Magnetic Exchange Interaction via N-H···O-Bonding in Copper(II) Complex with 1-Phenyl-3-Methyl-4-Formylpyrazol-5-One 2-Quinolylhydrazone. *Inorganica Chim. Acta* **2013**, *405*, 169–175.

(38) Cha, S. J.; Kim, K. Effects of the Edaravone, a Drug Approved for the Treatment of Amyotrophic Lateral Sclerosis, on Mitochondrial Function and Neuroprotection. *Antioxidants* **2022**, *11*, 195.

(39) Pettinari, R.; Marchetti, F.; Di Nicola, C.; Pettinari, C.; Galindo, A.; Petrelli, R.; Cappellacci, L.; Cuccioloni, M.; Bonfili, L.; Eleuteri, A. M.; Guedes Da Silva, M. F. C.; Pombeiro, A. J. L. Ligand Design for N, O- or N, N-Pyrazolone-Based Hydrazones Ruthenium(II)-Arene Complexes and Investigation of Their Anticancer Activity. *Inorg. Chem.* **2018**, *57*, 14123–14133.

(40) Cuccioloni, M.; Bonfili, L.; Cecarini, V.; Nabissi, M.; Pettinari, R.; Marchetti, F.; Petrelli, R.; Cappellacci, L.; Angeletti, M.; Eleuteri, A. M. Exploring the Molecular Mechanisms Underlying the in Vitro Anticancer Effects of Multitarget-Directed Hydrazone Ruthenium(II)–Arene Complexes. *ChemMedChem.* **2020**, *15*, 105–113.

(41) Zhang, P.; Zhang, L.; Wang, C.; Xue, S.; Lin, S. Y.; Tang, J. Equatorially Coordinated Lanthanide Single Ion Magnets. *J. Am. Chem. Soc.* **2014**, *136*, 4484–4487.

(42) Casanova, D.; Llunell, M.; Alemany, P.; Alvarez, S. The Rich Stereochemistry of Eight-Vertex Polyhedra: A Continuous Shape Measures Study. *Chem. Eur. J.* **2005**, *11*, 1479–1494.

(43) Ruiz-Martínez, A.; Casanova, D.; Alvarez, S. Polyhedral Structures with an Odd Number of Vertices: Nine-Coordinate Metal Compounds. *Chem. Eur. J.* **2008**, *14*, 1291–1303.

(44) Reta, D.; Chilton, N. F. Uncertainty Estimates for Magnetic Relaxation Times and Magnetic Relaxation Parameters. *Phys. Chem. Chem. Phys.* **2019**, *21*, 23567–23575.

(45) Guo, F. S.; He, M.; Huang, G. Z.; Giblin, S. R.; Billington, D.; Heinemann, F. W.; Tong, M. L.; Mansikkamäki, A.; Layfield, R. A. Discovery of a Dysprosium Metallocene Single-Molecule Magnet with Two High-Temperature Orbach Processes. *Inorg. Chem.* **2022**, *61*, 6017–6025.

(46) Gupta, S. K.; Dey, S.; Rajeshkumar, T.; Rajaraman, G.; Murugavel, R. Deciphering the Role of Anions and Secondary Coordination Sphere in Tuning Anisotropy in Dy(III) Air-Stable D_{5h} SIMs. *Chem. Eur. J.* **2021**, *27*, 1–12.

(47) Parmar, V. S.; Mills, D. P.; Winpenny, R. E. P. Mononuclear Dysprosium Alkoxide and Aryloxide Single-Molecule Magnets. *Chem. Eur. J.* **2021**, *27*, 7625–7645.

(48) Jensen, B. S. The Synthesis of 1-Phenyl-3-Methyl-4-Acyl-Pyrazolones-5. *Acta Chem. Scand.* **1959**, *13*, 1668–1670.

"For Table of Contents Use Only"

Edaravone based mononuclear dysprosium(III) single-molecule magnets

Tesfay G. Ashebr,[†, ‡, #] Léo La Droitte,[§] Xiao-Lei Li,[†] Chen Zhao,[†, ‡] Jinjiang Wu,[†, ‡] Quan Zhou,[†, ‡] Olivier Cador,[§] Boris Le Guennic*[, §] and Jinkui Tang*[, †, ‡]

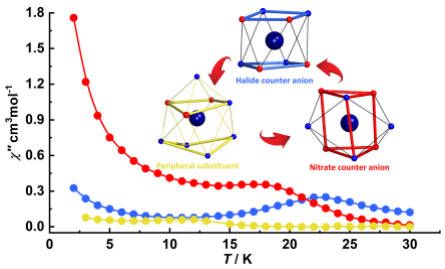

The magnetic properties of first edaravone-based mononuclear Dy(III) single-molecule magnets (SMMs) were subtly tuned through chemical modifications on the dominant crystal-field interaction.